

Time-Correlated Video Bridge Matching

Viacheslav Vasilev¹

Arseny Ivanov²

Nikita Gushchin²

Maria Kovaleva¹

Alexander Korotin²

¹FusionBrain Lab

²Applied AI Institute

Abstract

Diffusion models excel in noise-to-data generation tasks, providing a mapping from a Gaussian distribution to a more complex data distribution. However they struggle to model translations between complex distributions, limiting their effectiveness in data-to-data tasks. While Bridge Matching (BM) models address this by finding the translation between data distributions, their application to time-correlated data sequences remains unexplored. This is a critical limitation for video generation and manipulation tasks, where maintaining temporal coherence is particularly important. To address this gap, we propose Time-Correlated Video Bridge Matching (TCVBM), a framework that extends BM to time-correlated data sequences in the video domain. TCVBM explicitly models inter-sequence dependencies within the diffusion bridge, directly incorporating temporal correlations into the sampling process. We compare our approach to classical methods based on bridge matching and diffusion models for three video-related tasks: frame interpolation, image-to-video generation, and video super-resolution. TCVBM achieves superior performance across multiple quantitative metrics, demonstrating enhanced generation quality and reconstruction fidelity.

1 INTRODUCTION

Diffusion models (Sohl-Dickstein et al., 2015; Ho et al., 2020; Song et al., 2021b) have emerged as a powerful paradigm for generative modeling, achieving remarkable results in high-fidelity data synthesis (Saharia et al., 2022; Rombach et al., 2022; Arkhipkin

et al., 2024; Labs, 2024). By iteratively denoising samples from a Gaussian distribution, these models excel at producing diverse and realistic outputs. However, despite their widespread adoption, diffusion models exhibit a critical limitation: they struggle to model translations between complex-structured data distributions. This shortcoming hinders their effectiveness in data-to-data tasks, where smooth bridging of the distributions is essential.

In contrast, Bridge Matching (BM) offers a principled solution to this problem by explicitly constructing a translation between arbitrary data distributions (Peluchetti, 2023b,a; Liu et al., 2022; Zhou et al., 2023). These methods learn vector field that connects source and target distributions, demonstrating strong performance in image-to-image tasks (Shi et al., 2023; Liu et al., 2023). However, the translation between independent data sequences, the components of which are time-correlated, remains unaddressed. At the same time, this is exactly what video data is, where one data sample is a sequence of correlated frames. While existing methods assume to operate with video data samples without considering their internal structure (Wang et al., 2025b), this omission can lead to a decrease in temporal consistency in the generated video.

Contribution. To address these issues, we propose Time-Correlated Video Bridge Matching (TCVBM), a novel framework that extends Bridge Matching to time-dependent video data. Unlike prior work, TCVBM explicitly takes into account inter-sequence dependencies, ensuring faithful translation between source and target distributions (Figure 1). We evaluate TCVBM on three video-related tasks: frame interpolation, image-to-video generation, and video super resolution. A comparison with classical approaches that do not take into account the correlation between frames, such as DDPM (Ho et al., 2020), DDIM (Song et al., 2021a), and Bridge Matching, demonstrates that TCVBM provides better temporal consistency and reconstruction quality.

2 RELATED WORKS

2.1 Bridge Models

Despite the widespread adoption of diffusion models in generative tasks (Sohl-Dickstein et al., 2015; Ho et al., 2020; Song et al., 2021b), the Gaussian noise commonly used to initialize the generation process lacks meaningful structural information about the underlying data distribution. However, by matching the velocity fields with pre-defined transport maps, it is possible to construct powerful generative models that rival diffusion-based approaches (Lipman et al., 2023). Furthermore, Diffusion Bridge Models have been shown to provide a more flexible framework for generative tasks compared to standard diffusion processes (Bortoli et al., 2021; Liu et al., 2022). Particularly, bridge models have shown their superiority over diffusion baselines for image restoration (Delbracio and Milanfar, 2024), image translation (Zhou et al., 2024a), and image reconstruction (Liu et al., 2023). Despite this, the use of Bridge Matching to work with complex distributions of sequential data, the components of which are correlated, remains a practically unexplored topic. A recent attempt to extend Bridge Matching to image-to-video generation, overlooked the intrinsic temporal dependencies between video frames (Wang et al., 2025b). In our solution, we address this problem and design our own interpolant that explicitly accounts for the assumption of linear correlations among the components of the random vectors that represent video data samples.

2.2 Video Generation and Manipulation

Here, we provide a brief overview of the methods for some video-related tasks. Without loss of generality, we evaluate the applicability of our approach to the video domain using the following three tasks:

Frame Interpolation aims to synthesize middle frames between two input images while ensuring temporal smoothness and content consistency. Traditional approaches often rely on optical flow estimation between keyframes (Niklaus and Liu, 2020; Lee et al., 2020; Park et al., 2021; Huang et al., 2022) or leverage convolutional features and attention maps for middle frame generation (Kalluri et al., 2023; Shi et al., 2022; Reda et al., 2022). Diffusion models were first used for video interpolation using bidirectional masking to synthesize middle frames (Voleti et al., 2022). Subsequent advances expanded this direction, including conditional diffusion-based generation (Danier et al., 2024), multi-stage cascaded refinement (Jain et al., 2024), adapted image-to-video diffusion models (Wang et al., 2025a), and techniques for large-motion gener-

ation (Shen et al., 2024). However, these methods do not explicitly model inter-frame correlations in video sequences. Similarly, event-based approaches (Chen et al., 2025; Zhang et al., 2025) incorporate additional motion cues but still rely on standard diffusion processes without accounting for temporal correlations.

Image-to-Video Generation is a specific type of video generation, where an image is used as the input for a neural network, which then creates a video with consistent and semantically accurate movement. Diffusion models and recent advancements in generative architectures have taken this task to a new level, providing high-quality results (Zhang et al., 2023; Xing et al., 2023; Shi et al., 2024; Guo et al., 2023, 2024; Arkhipkin et al., 2025). However, the fundamental limitation of the diffusion process on the noise-to-data setup posed a risk of losing essential information that must be transferred from the image to the animated video. Different approaches tried to solve this without going beyond the diffusion process (Ren et al., 2024; Wu et al., 2023), until FrameBridge (Wang et al., 2025b) proposed an approach for image-to-video generation based on Bridge Matching. FrameBridge uses the input image as a prior instead of the Gaussian distribution used in the diffusion algorithm. Although this makes it reasonable to consider the image-to-video generation as a data-to-data task, this approach does not take into account the specifics of the internal video data structure, in fact adapting bridge matching algorithm from image to video domain. In this paper, we propose a method that explicitly assumes the correlation of frames with each other and uses this to obtain samples from bridge distribution.

Video Super Resolution focuses on reconstructing high-resolution video frames from their degraded low-resolution versions. The application of diffusion models to this task is motivated by their strong generative prior, which is capable of synthesizing realistic details to overcome complex degradations. A central challenge is reconciling the stochastic nature of the diffusion process with the stringent requirement for temporal coherence across video frames. To resolve this, methods such as Upscale-A-Video (Zhou et al., 2024b) and MGLD (Yang et al., 2024) introduce explicit spatiotemporal constraints, using techniques like temporal layer integration and motion-guided loss optimization. At the same time, bridge-matching methods have been applied for super resolution in the image domain (Liu et al., 2023; Gushchin et al., 2025). In this work, we expand the application of these methods to video super resolution and propose a new approach that explicitly accounts for temporal coherence between video frames.

3 BACKGROUND ON BRIDGE MATCHING

We briefly review the Bridge Matching framework (Peluchetti, 2023b,a; Liu et al., 2022; Shi et al., 2023), which constructs diffusion processes for data translation, given a distribution of clean data $p(\mathbf{x}_0)$ and corrupted data $p(\mathbf{x}_T)$ on \mathbb{R}^D . The goal is to model a stochastic process that transitions from $\mathbf{x}_0 \sim p(\mathbf{x}_0)$ to $\mathbf{x}_T \sim p(\mathbf{x}_T | \mathbf{x}_0)$, while incorporating a prior dynamics.

Consider a coupling $p(\mathbf{x}_0, \mathbf{x}_T) = p(\mathbf{x}_0)p(\mathbf{x}_T | \mathbf{x}_0)$, and let the prior process be defined by the stochastic differential equation (SDE):

$$d\mathbf{x}_t = f(\mathbf{x}_t, t) dt + g(t) d\mathbf{W}_t, \quad (1)$$

where $f(\mathbf{x}_t, t)$ is a drift function, $g(t)$ is a time-dependent noise scale, and \mathbf{W}_t is a standard Wiener process. For a fixed starting point \mathbf{x}_s , we denote the marginal of the prior process at time t by $q(\mathbf{x}_t | \mathbf{x}_s)$.

Bridge Distribution. Given a pair $(\mathbf{x}_0, \mathbf{x}_{t'})$ from the prior, the posterior distribution of the process at time $t < t'$, denoted as $q(\mathbf{x}_t | \mathbf{x}_0, \mathbf{x}_{t'})$, is referred to as the *bridge distribution*. Using Bayes' rule, it is expressed as:

$$q(\mathbf{x}_t | \mathbf{x}_0, \mathbf{x}_{t'}) = \frac{q(\mathbf{x}_{t'} | \mathbf{x}_t, \mathbf{x}_0) q(\mathbf{x}_t | \mathbf{x}_0)}{q(\mathbf{x}_{t'} | \mathbf{x}_0)}.$$

Bridge Matching Dynamics. Bridge Matching aims to construct a stochastic process that interpolates between \mathbf{x}_T and \mathbf{x}_0 using a reverse-time SDE:

$$d\mathbf{x}_t = \{f(\mathbf{x}_t, t) - g^2(t) v^*(\mathbf{x}_t, t)\} dt + g(t) d\bar{\mathbf{W}}_t,$$

where $\bar{\mathbf{W}}_t$ is a standard Wiener process under time reversal $t \leftarrow T - t$, and dt denotes a negative infinitesimal timestep.

Learning Objective. The drift function $v^*(\mathbf{x}_t, t)$ is approximated using the following optimization objective:

$$\min_{\phi} \mathbb{E}_{\mathbf{x}_0, \mathbf{x}_T, t} \left[\|v_{\phi}(\mathbf{x}_t, t) - \nabla_{\mathbf{x}_t} \log q(\mathbf{x}_t | \mathbf{x}_0)\|^2 \right], \quad (2)$$

where $\mathbf{x}_0 \sim p(\mathbf{x}_0)$, $\mathbf{x}_T \sim p(\mathbf{x}_T | \mathbf{x}_0)$, and $\mathbf{x}_t \sim q(\mathbf{x}_t | \mathbf{x}_0, \mathbf{x}_T)$ is sampled from the bridge distribution. Time t is sampled uniformly from the interval $[0, T]$.

This formulation provides a principled way to learn drift functions that guide the translation of corrupted data samples from $p(\mathbf{x}_T)$ to clean data samples from $p(\mathbf{x}_0)$ through learned diffusion processes.

4 METHOD

In this section, we introduce our proposed *Time-Correlated Video Bridge Matching (TCVBM)* method for modeling video data sequences. The core idea is to incorporate temporal correlations directly into the prior diffusion process, enabling better coherence and reconstruction of sequential data (Figure 1). We provide formal derivations and defer all proofs to the supplementary material section A.

4.1 Time-Correlated Prior Process

We consider sequences of length N , represented as

$$\mathbf{X} = (\mathbf{x}^1, \dots, \mathbf{x}^N), \quad (3)$$

where each $\mathbf{x}^n \in \mathbb{R}^D$ for $n = 1, \dots, N$. We aim to define a prior diffusion process that imposes an inductive bias toward temporal smoothness across elements.

Column-wise independence across features. To model high-dimensional data efficiently, we assume that the D feature dimensions evolve independently but share the same temporal dynamics. For each feature index $d = 1, \dots, D$, we define the time-dependent trajectory

$$\mathbf{x}_t^{(d)} = \begin{bmatrix} x_t^{(d,1)} & \dots & x_t^{(d,N)} \end{bmatrix}^{\top} \in \mathbb{R}^N,$$

which evolves by a stochastic differential equation (SDE):

$$d\mathbf{x}_t^{(d)} = (\mathbf{A}\mathbf{x}_t^{(d)} + \mathbf{b}^{(d)}) dt + g(t) d\mathbf{W}_t^{(d)},$$

where $\mathbf{A} \in \mathbb{R}^{N \times N}$ is a symmetric, invertible matrix encoding temporal correlations, $\mathbf{b}^{(d)} \in \mathbb{R}^N$ is a drift correction term, and $\mathbf{W}_t^{(d)}$ is a standard Wiener process.

Matrix form of the prior. Equivalently, the full intermediate sequence $\mathbf{X}_t \in \mathbb{R}^{N \times D}$ evolves as:

$$d\mathbf{X}_t = (\mathbf{A}\mathbf{X}_t + \mathbf{b}) dt + g(t) d\mathbf{W}_t,$$

where $\mathbf{b} = [\mathbf{b}^{(1)} \dots \mathbf{b}^{(D)}] \in \mathbb{R}^{N \times D}$, and $\mathbf{W}_t \in \mathbb{R}^{N \times D}$ is a matrix of independent Wiener processes across columns. In all expressions involving covariance and scores, formulas are applied column-wise. For example,

$$\Sigma_t^{-1}(\mathbf{X}_t - \boldsymbol{\mu}_t) \in \mathbb{R}^{N \times D}$$

denotes applying $\Sigma_t^{-1} \in \mathbb{R}^{N \times N}$ independently to each column of $\mathbf{X}_t - \boldsymbol{\mu}_t$. Further, unless otherwise stated, we will assume a time-independent noise scale $g(t) = \sqrt{\epsilon}$ for simplicity.

We now derive the transition and bridge distributions for this prior, which are essential for bridge matching.

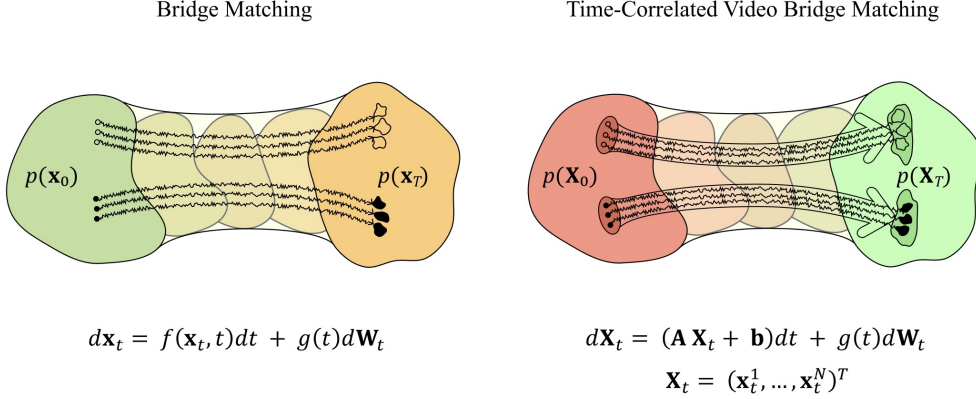


Figure 1: Comparison of the Bridge Matching and Time-Correlated Video Bridge Matching methods. The frames of the same video in the distributions $p(\mathbf{x}_0)$ and $p(\mathbf{X}_0)$ are indicated by dots of the same color. While Bridge Matching method makes the transition from one distribution to another without considering the relationship between frames, our approach treats one video as a single \mathbf{X}_0 data sequence and constructs the transition taking into account the internal correlation between video frames.

Proposition 1 (Correlated Process Score). *Let \mathbf{X}_t follow the linear SDE:*

$$d\mathbf{X}_t = (\mathbf{A}\mathbf{X}_t + \mathbf{b})dt + \sqrt{\epsilon}d\mathbf{W}_t, \quad \mathbf{X}_0 \sim \delta_{\mathbf{X}_0}, \quad (4)$$

then the marginal distribution of \mathbf{X}_t is Gaussian:

$$q(\mathbf{X}_t | \mathbf{X}_0) = \mathcal{N}(\mathbf{X}_t | \boldsymbol{\mu}_{t|0}(\mathbf{X}_0), \boldsymbol{\Sigma}_{t|0}), \quad (5)$$

with

$$\boldsymbol{\mu}_{t|0}(\mathbf{X}_0) = e^{\mathbf{A}t}\mathbf{X}_0 + (e^{\mathbf{A}t} - I)\mathbf{A}^{-1}\mathbf{b}, \quad (6)$$

$$\boldsymbol{\Sigma}_{t|0} = \epsilon \frac{e^{2\mathbf{A}t} - I}{2} \mathbf{A}^{-1}. \quad (7)$$

The score function is then given by

$$\nabla_{\mathbf{X}_t} \log q(\mathbf{X}_t | \mathbf{X}_0) = -\boldsymbol{\Sigma}_{t|0}^{-1}(\mathbf{X}_t - \boldsymbol{\mu}_{t|0}(\mathbf{X}_0)). \quad (8)$$

To perform bridge matching, one also needs to be able to sample from $q(\mathbf{X}_t | \mathbf{X}_0, \mathbf{X}_T)$.

Proposition 2 (Correlated Bridge Distribution). *Let \mathbf{X}_t follow the same SDE as in Proposition 1. Then, given fixed endpoints \mathbf{X}_0 and $\mathbf{X}_{t'}$, the posterior (bridge) distribution of \mathbf{X}_t is Gaussian:*

$$q(\mathbf{X}_t | \mathbf{X}_0, \mathbf{X}_{t'}) = \mathcal{N}(\mathbf{X}_t | \boldsymbol{\mu}_{t|0,t'}, \boldsymbol{\Sigma}_{t|0,t'}), \quad (9)$$

where

$$\boldsymbol{\mu}_{t|0,t'} = \boldsymbol{\mu}_{t|0}(\mathbf{X}_0) + \boldsymbol{\Sigma}_{t|0} \boldsymbol{\Sigma}_{t'|0}^{-1}(\mathbf{X}_{t'} - \boldsymbol{\mu}_{t'|0}(\mathbf{X}_0)), \quad (10)$$

$$\boldsymbol{\Sigma}_{t|0,t'} = \boldsymbol{\Sigma}_{t|0} - \boldsymbol{\Sigma}_{t|0} \boldsymbol{\Sigma}_{t'|0}^{-1} \boldsymbol{\Sigma}_{t|0}. \quad (11)$$

Together, Propositions 1 and 2 provide closed-form expressions required to implement bridge matching under the time-correlated prior.

4.2 Time-Correlated Video Bridge Matching

Training. To train a bridge matching model, we follow the general framework of Bridge Matching described in section 3. We assume access to clean samples $\mathbf{X}_0 \sim p_0(\mathbf{X}_0)$, and a degradation process $p(\mathbf{X}_T | \mathbf{X}_0)$, together forming a coupling $p(\mathbf{X}_0, \mathbf{X}_T) = p_0(\mathbf{X}_0)p(\mathbf{X}_T | \mathbf{X}_0)$.

We aim to minimize the squared error between the predicted score function $v_\phi(\mathbf{X}_t, t)$ and the score of prior process $\nabla_{\mathbf{X}_t} \log p(\mathbf{X}_t | \mathbf{X}_0)$, averaged over bridge samples $\mathbf{X}_t \sim p(\mathbf{X}_t | \mathbf{X}_0, \mathbf{X}_T)$:

$$\min_{\phi} \mathbb{E}_{\mathbf{X}_0, \mathbf{X}_t, t} \left[\left\| v_\phi(\mathbf{X}_t, t) + \boldsymbol{\Sigma}_{t|0}^{-1}(\mathbf{X}_t - \boldsymbol{\mu}_{t|0}(\mathbf{X}_0)) \right\|^2 \right], \quad (12)$$

where $t \sim \text{Uniform}(0, T)$.

This objective can be simplified by reparameterizing the score function in terms of an intermediate predictor:

Proposition 3 (Reparameterization of the drift function). *The minimizer $v^*(\mathbf{X}_t, t)$ of the objective (12) can be expressed as:*

$$v^*(\mathbf{X}_t, t) = -\boldsymbol{\Sigma}_{t|0}^{-1} \left(\mathbf{X}_t - \boldsymbol{\mu}_{t|0}(\widehat{\mathbf{X}}_0^*(\mathbf{X}_t, t)) \right),$$

where $\widehat{\mathbf{X}}_0^(\mathbf{X}_t, t)$ is the solution to the regression problem:*

$$\min_{\phi} \mathbb{E}_{\mathbf{X}_0, \mathbf{X}_t, t} \left[\left\| \widehat{\mathbf{X}}_0^*(\mathbf{X}_t, t) - \mathbf{X}_0 \right\|^2 \right]. \quad (13)$$

Thus, learning the score function reduces to learning a predictor for the clean data \mathbf{X}_0 .

We parameterize the predictor $\widehat{\mathbf{X}}_0^*(\mathbf{X}_t, t)$ with a neural network and train it using the regression loss in (13). The training procedure is summarized in Algorithm 1.

Algorithm 1 Training

Require: data from coupling $p_0(\mathbf{X}_0)p_T(\mathbf{X}_T|\mathbf{X}_0)$ and coefficients \mathbf{A} , \mathbf{b} and ϵ for prior (1).

- 1: **repeat**
- 2: $t \sim \mathcal{U}([0, 1])$, $\mathbf{X}_0 \sim p_0(\mathbf{X}_0)$, $\mathbf{X}_T \sim p(\mathbf{X}_T | \mathbf{X}_0)$
- 3: $\mathbf{X}_t \sim q(\mathbf{X}_t | \mathbf{X}_0, \mathbf{X}_T)$ (9)
- 4: Take gradient descent step on $\mathbf{X}_0^\phi(\mathbf{X}_t, t)$ (13)
- 5: **until** convergence

Algorithm 2 Inference

Require: Input $\mathbf{X}_T \sim p_T(\mathbf{X}_T)$, trained model $\widehat{\mathbf{X}}_0^\phi(\cdot, \cdot)$, time schedule $\{t_n\}_{n=0}^N$

- 1: Set $\mathbf{X}_{t_N} \leftarrow \mathbf{X}_T$
- 2: **for** $n = N$ **to** 1 **do**
- 3: Predict $\widehat{\mathbf{X}}_0 \leftarrow \widehat{\mathbf{X}}_0^\phi(\mathbf{X}_{t_n}, t_n)$
- 4: Sample $\mathbf{X}_{t_{n-1}} \sim p(\mathbf{X}_{t_{n-1}} | \widehat{\mathbf{X}}_0, \mathbf{X}_{t_n})$ using (9)
- 5: **end for**
- 6: **return** $\mathbf{X}_0 = \mathbf{X}_{t_0}$

Inference. At inference time, given a corrupted sequence $\mathbf{X}_T \sim p(\mathbf{X}_T)$, we perform iterative denoising using the learned predictor and the time-correlated bridge distribution. Given a schedule $0 = t_0 < t_1 < \dots < t_N = T$, we iteratively refine the estimate of \mathbf{X}_0 by sampling from posterior:

$$\mathbf{X}_{t_{n-1}} \sim p(\mathbf{X}_{t_{n-1}} | \widehat{\mathbf{X}}_0, \mathbf{X}_{t_n}),$$

where $\widehat{\mathbf{X}}_0 = \widehat{\mathbf{X}}_0^\phi(\mathbf{X}_{t_n}, t_n)$ obtained by using prediction of the trained model. This process is detailed in Algorithm 2.

4.3 Choice of the Prior Process for Video Manipulation Tasks

To encourage smooth transitions between consecutive elements of the sequence, we define the prior matrix \mathbf{A} of the size $N \times N$ with a tridiagonal structure:

$$\mathbf{A} = \begin{bmatrix} -2 & 1 & 0 & \cdots & 0 \\ 1 & -2 & 1 & \ddots & \vdots \\ 0 & \ddots & \ddots & \ddots & 0 \\ \vdots & \ddots & 1 & -2 & 1 \\ 0 & \cdots & 0 & 1 & -2 \end{bmatrix}.$$

Here, \mathbf{A} promotes temporal correlations across adjacent elements, and the per-element prior is:

$$d\mathbf{x}_t^n = ((\mathbf{x}_t^{n-1} - \mathbf{x}_t^n) + (\mathbf{x}_t^{n+1} - \mathbf{x}_t^n)) dt + \sqrt{\epsilon} d\mathbf{W}_t, \quad (14)$$

where $n = 2, \dots, N - 1$. This formulation naturally encourages a linear relationship between the elements

of the sequence. From the point of view of this approximation, each frame \mathbf{x}_t^n should remain close to the average of its neighbors \mathbf{x}_t^{n-1} and \mathbf{x}_t^{n+1} . It is particularly well-suited for video-related tasks, where the frames of one video are correlated with each other, and the prior process enforces consistency and smoothness between them.

Depending on the video manipulation task, we suggest the following options for vector \mathbf{b} and equation 14:

Frame Interpolation. In this case, we consider the sequence of length $N + 2$, represented as

$$\tilde{\mathbf{X}} = (\mathbf{x}^0, \mathbf{x}^1, \dots, \mathbf{x}^N, \mathbf{x}^{N+1}),$$

where the endpoints \mathbf{x}^0 and \mathbf{x}^{N+1} are fixed as the initial and final frames of a video clip, between which it is necessary to make interpolation. The middle part of the video will be defined in the same way as in the equation 3:

$$\mathbf{X} = (\mathbf{x}^1, \dots, \mathbf{x}^N),$$

and all statements for \mathbf{X}_t from paragraphs 4.1 and 4.2 remain valid. Considering in equation 14 for all t and $n = 1, \dots, N$ $\mathbf{x}_t^0 = \mathbf{x}^0$ and $\mathbf{x}_t^{N+1} = \mathbf{x}^{N+1}$, we can define the vector \mathbf{b} as:

$$\mathbf{b} = [\mathbf{x}^0, 0, \dots, 0, \mathbf{x}^{N+1}]^T, \quad \mathbf{b} \in \mathbb{R}^{N \times D},$$

i.e. \mathbf{b} enforces the boundary conditions from the known fixed endpoints \mathbf{x}^0 and \mathbf{x}^{N+1} .

Image-to-Video Generation. This task corresponds to the case of one fixed left point of the video sequence, i.e.:

$$\tilde{\mathbf{X}} = (\mathbf{x}^0, \mathbf{x}^1, \dots, \mathbf{x}^N), \quad \tilde{\mathbf{X}} \in \mathbb{R}^{(N+1) \times D}$$

$$\mathbf{b} = [\mathbf{x}^0, 0, \dots, 0]^T, \quad \mathbf{b} \in \mathbb{R}^{N \times D},$$

and in the equation 14 for all n and t $\mathbf{x}_t^0 = \mathbf{x}^0$ and $\mathbf{x}_t^{N+1} = 0$.

Video Super Resolution. This is the simplest case, where $\tilde{\mathbf{X}} = \mathbf{X} \in \mathbb{R}^{N \times D}$, i.e. the endpoints are not fixed, and the vector \mathbf{b} is equal to zero.

5 EXPERIMENTS

5.1 Implementation Details

To evaluate the performance of our new method and compare it to other approaches, we take our own small and simple U-Net model based on several residual blocks with $2D$ convolutions. The model has approximately 8.7 million parameters. We conduct experiments on the MovingMNIST dataset (Srivastava

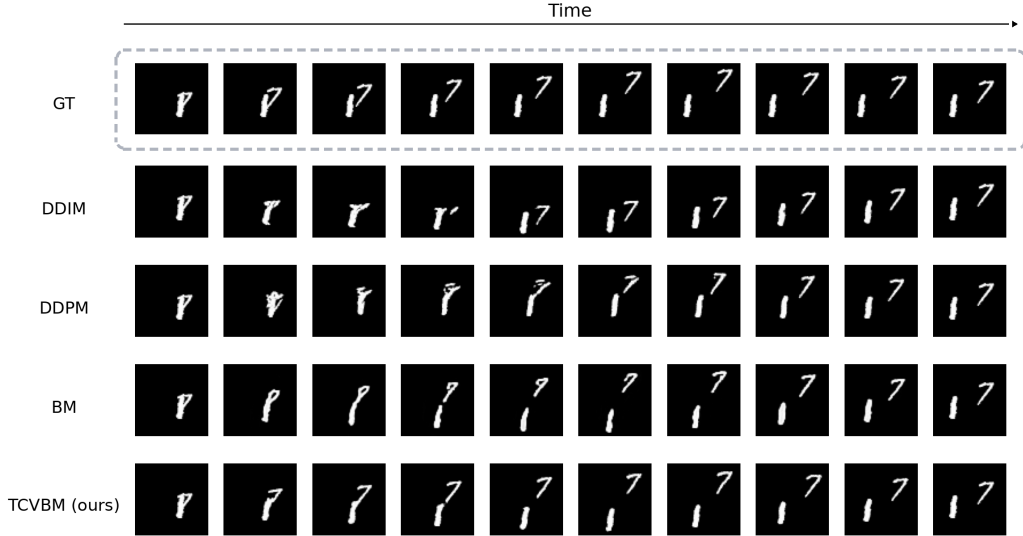


Figure 2: Frame interpolation results. The first and last frames are fixed and come from the dataset. The task is to generate the intermediate 8 frames. TCVBM provides a smoother and more consistent transition from frame to frame and a better detailization.

Table 1: Frame interpolation quantitative results.

Metric	FVD \downarrow	LPIPS \downarrow	PSNR \uparrow	SSIM \uparrow
DDIM	33.609	0.105	15.800	0.760
DDPM	32.404	0.117	14.937	0.741
BM	34.315	0.079	17.103	0.794
TCVBM (ours)	30.542	0.077	17.280	0.813

et al., 2015), which contains 10,000 video sequences each 20 frames long and showing 2 moving digits in a 64×64 resolution. For each experiment, we extract sub-sequences from the videos, consisting of 10 consecutive frames, and concatenate them into a 10-channel input for the neural network. We use 9,500 training sequences and 500 validation sequences, with a random split for each seed value. We train each model for 150,000 iterations with a batch size of 128 and an ema rate of 0.999. We use the AdamW optimizer (Loshchilov and Hutter, 2019) with betas set to 0.9 and 0.95, a weight decay of 10^{-4} , and a learning rate of 3×10^{-5} . The number of steps in the reverse process for all methods is equal to 1000. All experiments are conducted using a single NVIDIA Tesla A100 GPU.

5.2 Experiments Roadmap

We compare TCVBM with three classical generative methods: DDPM (Ho et al., 2020), DDIM (Song et al., 2021a), and Bridge Matching with Brownian Bridge (BM) (Ibe, 2013, Chapter 9). For each method, we use the same setup, except for the loss function and sam-

pling procedure in the forward and reverse processes, which are determined by the specific paradigm of each algorithm. Based on each of these four approaches, we train three models to solve the following tasks:

Frame Interpolation. A sequence of 10 frames is fed into the network as input, with the first and last frames from the dataset fixed. At the output, 8 middle frames are generated, which are then compared with 8 corresponding video frames from the dataset. The DDPM and DDIM methods aim to solve the generation problem for middle frames from random noise in the reverse process. For BM and TCVBM methods, we consider two ways to initialize the middle input frames: linear interpolation between the two fixed boundary frames, or noise samples from the Gaussian distribution $\mathcal{N}(\mathbf{0}, \mathbf{I})$. The second approach produced better results for BM and TCVBM, so the results presented here further are for noise-based initialization method. For more details, please see the Appendix C.1.

Image-to-Video Generation. The task is to generate the remaining 9 frames based on the first frame. We provide the first frame as input data, along with

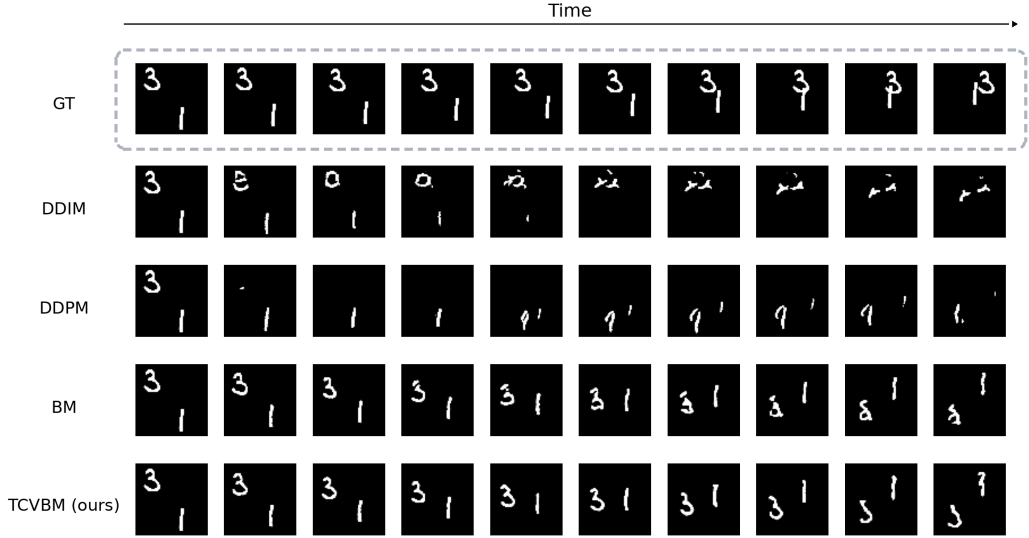


Figure 3: Image-to-Video generation results. Based on the first frame, the methods need to generate the next 9 frames. As can be seen, TCVBM makes it possible to achieve better appearance of the generations and a lower quality degradation with increasing sequence length.

Table 2: Image-to-Video generation quantitative results.

Metric	FVD \downarrow	LPIPS \downarrow	PSNR \uparrow	SSIM \uparrow
DDIM	77.72	0.294	10.88	0.603
DDPM	75.86	0.311	10.72	0.595
BM	49.32	0.271	10.63	0.579
TCVBM (ours)	44.96	0.258	10.75	0.591

9 Gaussian samples from $\mathcal{N}(\mathbf{0}, \mathbf{I})$, or 9 copies of the first frame. The second option demonstrated the best results for all methods, so further we consider this initialization variant. For more information, please see the Appendix C.2.

Video Super Resolution. The network accepts 10 low resolution frames, and 10 frames with the dataset resolution are expected at the output. We consider starting with resolutions of 16×16 or 32×32 for all methods, but due to the simplicity of the task, we did not see any significant advantages for our method using the second option. Therefore, the further results are reported for the starting resolution of 16×16 . We also consider two initialization options: feeding the network with only low resolution data or low resolution data concatenated with Gaussian noise. Both approaches produced similar results, and here we use noise-free variant. More details can be found in the Appendix C.3.

Below, we present the results for the BM and TCVBM methods with ϵ equal to 0.1 and a coefficient at \mathbf{A} set to 1 for the TCVBM model, i.e., $\tilde{\mathbf{A}} = \alpha \mathbf{A}$ and

$\tilde{\mathbf{b}} = \alpha \mathbf{b}$, where $\alpha = 1$. Additionally, we conduct a series of experiments to find optimal hyperparameters ϵ and α . The results of these experiments can be found in Appendix D. Furthermore, we explored the dynamic correlation approach in which the coefficient α_t depends on time and increases as the reverse process progresses, i.e. when $t \rightarrow 0$. However, our experiments showed that this approach does not provide an advantage over TCVBM when the α is time-independent. The theoretical background and experimental findings are presented in Appendix E.

5.3 Results

Qualitative Comparison. As can be seen in Figures 2, 3, and 4, TCVBM produces more consistent and accurate results compared to other generative methods. By considering the mutual correlation between frames, our approach ensures a smoother transition and information transfer between them, which enhances the overall method stability. Additional examples can be found in Appendix F.

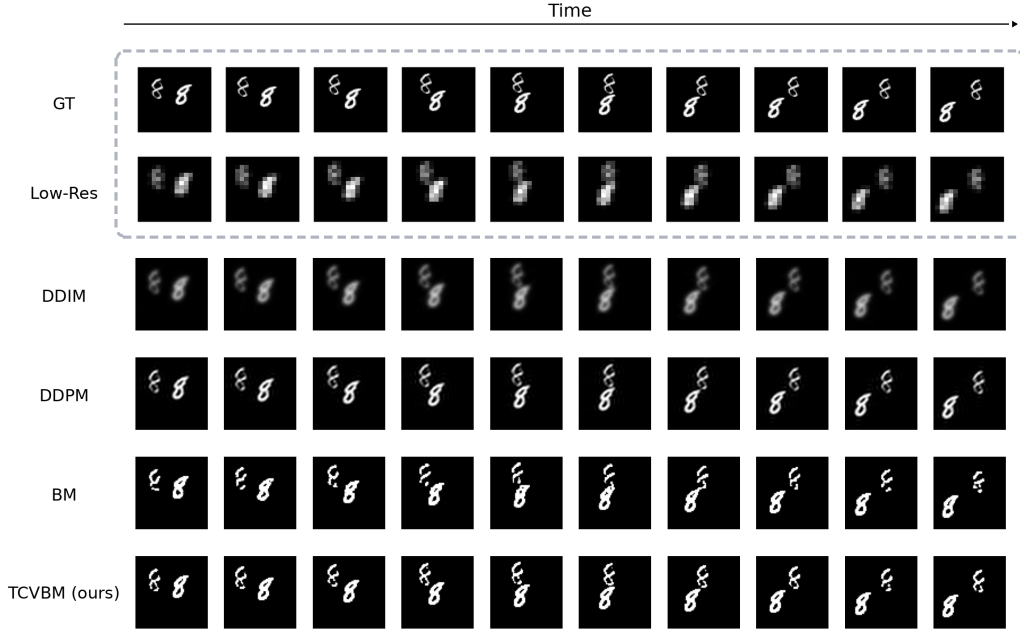


Figure 4: Video super resolution results. The resolution is increased from 16×16 to 64×64 . As can be seen, TCVBM outperforms other methods.

Table 3: Video super resolution quantitative results.

Metric	FVD \downarrow	LPIPS \downarrow	PSNR \uparrow	SSIM \uparrow
DDIM	334.700	0.514	17.307	0.613
DDPM	607.880	0.236	20.188	0.582
BM	53.516	0.020	22.642	0.954
TCVBM (ours)	59.491	0.020	22.670	0.970

Quantitative Evaluation. We perform quantitative evaluation on 500 videos from our MovingMNIST validation set using four metrics: FVD (Unterthiner et al., 2019), LPIPS (Zhang et al., 2018), PSNR, and SSIM. Tables 1, 2, and 3 present the metric values. As can be seen, in most cases TCVBM outperforms other approaches in terms of quantitative metrics. Additional results providing the standard deviation over launches with different random seeds are presented in the Appendix B.

6 DISCUSSION

Potential Impact. The proposed Time-Correlated Video Bridge Matching (TCVBM) framework is designed for generative modeling and manipulation with sequential video data. Unlike traditional diffusion and bridge matching methods, which often ignore the intrinsic temporal structure of data, TCVBM explicitly models inter-sequence correlations. This principle are applicable not only to video but also to other types of sequences, such as audio signals or time series, where

temporal consistency is important. The flexibility in defining prior process parameters, such as tridiagonal matrices for local correlations, allows for the method to be adapted to specific applications.

Limitations. This work has several limitations. First, the reliance on a predefined tridiagonal matrix prior is likely insufficient for capturing the complex nature of temporal dependencies in real-world data, particularly long-range and non-linear dynamics. Consequently, the exploration of more sophisticated interpolants – potentially modeling correlations in a feature space via adapters rather than directly between frames-is a critical direction for future work. Second, the computational cost of the iterative sampling process precludes real-time application. Finally, while the proposed approach offers a novel theoretical framework, its empirical validation is currently limited to the MovingMNIST dataset. Broader evaluation on large-scale, real-world datasets, complemented by human evaluation, is essential to substantiate its practical effectiveness and robustness.

References

Vladimir Arkhipkin, Vasilev Viacheslav, Filatov Andrei, Pavlov Igor, Agafonova Julia, Gerasimenko Nikolai, Averchenkova Anna, Mironova Evelina, Anton Bukashkin, Kulikov Konstantin, Kuznetsov Andrey, and Dimitrov Denis. Kandinsky 3: Text-to-image synthesis for multifunctional generative framework. In Delia Irazu Hernandez Farias, Tom Hope, and Manling Li, editors, *Proceedings of the 2024 Conference on Empirical Methods in Natural Language Processing: System Demonstrations*, pages 475–485, Miami, Florida, USA, November 2024. Association for Computational Linguistics. doi: 10.18653/v1/2024.emnlp-demo.48. URL <https://aclanthology.org/2024.emnlp-demo.48/>.

Vladimir Arkhipkin, Zein Shaheen, Viacheslav Vasilev, Elizaveta Dakhova, Konstantin Sobolev, Andrey Kuznetsov, and Denis Dimitrov. Improveyourvideos: Architectural improvements for text-to-video generation pipeline. *IEEE Access*, 13:1986–2003, 2025. doi: 10.1109/ACCESS.2024.3522510.

Valentin De Bortoli, James Thornton, Jeremy Heng, and Arnaud Doucet. Diffusion schrödinger bridge with applications to score-based generative modeling. In A. Beygelzimer, Y. Dauphin, P. Liang, and J. Wortman Vaughan, editors, *Advances in Neural Information Processing Systems*, 2021. URL <https://openreview.net/forum?id=9BnCwiXB0ty>.

Jingxi Chen, Brandon Y. Feng, Haoming Cai, Tianfu Wang, Levi Burner, Dehao Yuan, Cornelia Fermüller, Christopher A. Metzler, and Yiannis Aloimonos. Repurposing pre-trained video diffusion models for event-based video interpolation, 2025. URL <https://arxiv.org/abs/2412.07761>.

Duolikun Danier, Fan Zhang, and David Bull. Ldmvfi: video frame interpolation with latent diffusion models. In *Proceedings of the Thirty-Eighth AAAI Conference on Artificial Intelligence and Thirty-Sixth Conference on Innovative Applications of Artificial Intelligence and Fourteenth Symposium on Educational Advances in Artificial Intelligence, AAAI'24/IAAI'24/EAAI'24*. AAAI Press, 2024. ISBN 978-1-57735-887-9. doi: 10.1609/aaai.v38i2.27912. URL <https://doi.org/10.1609/aaai.v38i2.27912>.

Mauricio Delbracio and Peyman Milanfar. Inversion by direct iteration: An alternative to denoising diffusion for image restoration, 2024. URL <https://arxiv.org/abs/2303.11435>.

Xun Guo, Mingwu Zheng, Liang Hou, Yuan Gao, Yufan Deng, Pengfei Wan, Di Zhang, Yufan Liu, Weiming Hu, Zhengjun Zha, Haibin Huang, and Chongyang Ma. I2v-adapter: A general image-to-video adapter for diffusion models, 2024. URL <https://arxiv.org/abs/2312.16693>.

Yuwei Guo, Ceyuan Yang, Anyi Rao, Zhengyang Liang, Yaohui Wang, Yu Qiao, Maneesh Agrawala, Dahua Lin, and Bo Dai. Animatediff: Animate your personalized text-to-image diffusion models without specific tuning, 2023.

Nikita Gushchin, David Li, Daniil Selikhanovich, Evgeny Burnaev, Dmitry Baranchuk, and Alexander Korotin. Inverse bridge matching distillation, 2025. URL <https://arxiv.org/abs/2502.01362>.

Jonathan Ho, Ajay Jain, and Pieter Abbeel. Denoising diffusion probabilistic models. In *Proceedings of the 34th International Conference on Neural Information Processing Systems*, NIPS '20, Red Hook, NY, USA, 2020. Curran Associates Inc. ISBN 9781713829546.

Zhewei Huang, Tianyuan Zhang, Wen Heng, Boxin Shi, and Shuchang Zhou. Real-time intermediate flow estimation for video frame interpolation. In *Proceedings of the European Conference on Computer Vision (ECCV)*, 2022.

Oliver Ibe. *Markov processes for stochastic modeling*. Newnes, 2013.

Siddhant Jain, Daniel Watson, Eric Tabellion, Aleksander Hołyński, Ben Poole, and Janne Kontkanen. Video interpolation with diffusion models, 2024. URL <https://arxiv.org/abs/2404.01203>.

Tarun Kalluri, Deepak Pathak, Manmohan Chandraker, and Du Tran. Flavr: Flow-agnostic video representations for fast frame interpolation. In *2023 IEEE/CVF Winter Conference on Applications of Computer Vision (WACV)*, pages 2070–2081, 2023. doi: 10.1109/WACV56688.2023.00211.

Black Forest Labs. Flux. <https://github.com/black-forest-labs/flux>, 2024.

Hyeongmin Lee, Taeoh Kim, Tae-young Chung, Dae-hyun Pak, Yuseok Ban, and Sangyoun Lee. Adacof: Adaptive collaboration of flows for video frame interpolation. In *Proceedings of the IEEE/CVF Conference on Computer Vision and Pattern Recognition (CVPR)*, 2020.

Yaron Lipman, Ricky T. Q. Chen, Heli Ben-Hamu, Maximilian Nickel, and Matthew Le. Flow matching for generative modeling. In *The Eleventh International Conference on Learning Representations*, 2023. URL <https://openreview.net/forum?id=PqyMRDCJT9t>.

Guan-Horng Liu, Arash Vahdat, De-An Huang, Evangelos A. Theodorou, Weili Nie, and Anima Anandkumar. I2sb: image-to-image schrödinger bridge. In

Proceedings of the 40th International Conference on Machine Learning, ICML’23. JMLR.org, 2023.

Xingchao Liu, Lemeng Wu, Mao Ye, and qiang liu. Let us build bridges: Understanding and extending diffusion generative models. In *NeurIPS 2022 Workshop on Score-Based Methods*, 2022. URL <https://openreview.net/forum?id=0ef0CRKC9uZ>.

Ilya Loshchilov and Frank Hutter. Decoupled weight decay regularization. In *International Conference on Learning Representations*, 2019. URL <https://openreview.net/forum?id=Bkg6RiCqY7>.

Simon Niklaus and Feng Liu. Softmax splatting for video frame interpolation. In *IEEE Conference on Computer Vision and Pattern Recognition*, 2020.

Junheum Park, Chul Lee, and Chang-Su Kim. Asymmetric bilateral motion estimation for video frame interpolation. In *International Conference on Computer Vision*, 2021.

Stefano Peluchetti. Diffusion bridge mixture transports, schrödinger bridge problems and generative modeling. *Journal of Machine Learning Research*, 24(374):1–51, 2023a.

Stefano Peluchetti. Non-denoising forward-time diffusions. *arXiv preprint arXiv:2312.14589*, 2023b.

Kaare Brandt Petersen, Michael Syskind Pedersen, et al. The matrix cookbook. *Technical University of Denmark*, 7(15):510, 2008.

Fitsum Reda, Janne Kontkanen, Eric Tabellion, Deqing Sun, Caroline Pantofaru, and Brian Curless. Film: Frame interpolation for large motion. In *European Conference on Computer Vision (ECCV)*, 2022.

Weiming Ren, Harry Yang, Ge Zhang, Cong Wei, Xinrun Du, Stephen Huang, and Wenhui Chen. Consisti2v: Enhancing visual consistency for image-to-video generation. *arXiv preprint arXiv:2402.04324*, 2024.

Robin Rombach, Andreas Blattmann, Dominik Lorenz, Patrick Esser, and Björn Ommer. High-resolution image synthesis with latent diffusion models, 2022. URL <https://arxiv.org/abs/2112.10752>.

Chitwan Saharia, William Chan, Saurabh Saxena, Lala Li, Jay Whang, Emily Denton, Seyed Kamalar Seyed Ghasemipour, Burcu Karagol Ayan, S. Sara Mahdavi, Rapha Gontijo Lopes, Tim Salimans, Jonathan Ho, David J Fleet, and Mohammad Norouzi. Photorealistic text-to-image diffusion models with deep language understanding, 2022. URL <https://arxiv.org/abs/2205.11487>.

Liao Shen, Tianqi Liu, Huiqiang Sun, Xinyi Ye, Baopu Li, Jianming Zhang, and Zhiguo Cao. Dreammover: Leveraging the prior of diffusion models for image interpolation with large motion. In *Computer Vision – ECCV 2024: 18th European Conference, Milan, Italy, September 29–October 4, 2024, Proceedings, Part XV*, page 336–353, Berlin, Heidelberg, 2024. Springer-Verlag. ISBN 978-3-031-72632-3. doi: 10.1007/978-3-031-72633-0_19. URL https://doi.org/10.1007/978-3-031-72633-0_19.

Xiaoyu Shi, Zhaoyang Huang, Fu-Yun Wang, Weikang Bian, Dasong Li, Yi Zhang, Manyuan Zhang, Ka Chun Cheung, Simon See, Hongwei Qin, et al. Motion-i2v: Consistent and controllable image-to-video generation with explicit motion modeling. *SIGGRAPH 2024*, 2024.

Yuyang Shi, Valentin De Bortoli, Andrew Campbell, and Arnaud Doucet. Diffusion schrödinger bridge matching. In *Thirty-seventh Conference on Neural Information Processing Systems*, 2023. URL <https://openreview.net/forum?id=qy070HsJT5>.

Zhihao Shi, Xiangyu Xu, Xiaohong Liu, Jun Chen, and Ming-Hsuan Yang. Video frame interpolation transformer. In *CVPR*, 2022.

Jascha Sohl-Dickstein, Eric Weiss, Niru Maheswaranathan, and Surya Ganguli. Deep unsupervised learning using nonequilibrium thermodynamics. In Francis Bach and David Blei, editors, *Proceedings of the 32nd International Conference on Machine Learning*, volume 37 of *Proceedings of Machine Learning Research*, pages 2256–2265, Lille, France, 07–09 Jul 2015. PMLR. URL <https://proceedings.mlr.press/v37/sohl-dickstein15.html>.

Jiaming Song, Chenlin Meng, and Stefano Ermon. Denoising diffusion implicit models. In *International Conference on Learning Representations*, 2021a. URL <https://openreview.net/forum?id=St1giarCHLP>.

Yang Song, Jascha Sohl-Dickstein, Diederik P Kingma, Abhishek Kumar, Stefano Ermon, and Ben Poole. Score-based generative modeling through stochastic differential equations. In *International Conference on Learning Representations*, 2021b. URL <https://openreview.net/forum?id=PxTIG12RRHS>.

Nitish Srivastava, Elman Mansimov, and Ruslan Salakhutdinov. Unsupervised learning of video representations using lstms. *CoRR*, abs/1502.04681, 2015. URL <http://arxiv.org/abs/1502.04681>.

Thomas Unterthiner, Sjoerd van Steenkiste, Karol Kurach, Raphael Marinier, Marcin Michalski, and Sylvain Gelly. Towards accurate generative models of video: A new metric & challenges, 2019. URL <https://arxiv.org/abs/1812.01717>.

Vikram Voleti, Alexia Jolicoeur-Martineau, and Christopher Pal. Mcvd: Masked conditional video diffusion for prediction, generation, and interpolation. In *(NeurIPS) Advances in Neural Information Processing Systems*, 2022. URL <https://arxiv.org/abs/2205.09853>.

Xiaojuan Wang, Boyang Zhou, Brian Curless, Ira Kemelmacher-Shlizerman, Aleksander Holynski, and Steve Seitz. Generative inbetweening: Adapting image-to-video models for keyframe interpolation. In *The Thirteenth International Conference on Learning Representations*, 2025a. URL <https://openreview.net/forum?id=ykD8a9gJvy>.

Yuji Wang, Zehua Chen, Chen Xiaoyu, Yixiang Wei, Jun Zhu, and Jianfei Chen. Framebridge: Improving image-to-video generation with bridge models. In *Forty-second International Conference on Machine Learning*, 2025b. URL <https://openreview.net/forum?id=iYmV2xRSNW>.

Tianxing Wu, Chenyang Si, Yuming Jiang, Ziqi Huang, and Ziwei Liu. Freeinit: Bridging initialization gap in video diffusion models. *arXiv preprint arXiv:2312.07537*, 2023.

Jinbo Xing, Menghan Xia, Yong Zhang, Haoxin Chen, Xintao Wang, Tien-Tsin Wong, and Ying Shan. Dynamicrafter: Animating open-domain images with video diffusion priors, 2023.

Xi Yang, Chenhang He, Jianqi Ma, and Lei Zhang. Motion-guided latent diffusion for temporally consistent real-world video super-resolution, 2024. URL <https://arxiv.org/abs/2312.00853>.

Guozhen Zhang, Yuhang Zhu, Yutao Cui, Xiaotong Zhao, Kai Ma, and Limin Wang. Motion-aware generative frame interpolation, 2025. URL <https://arxiv.org/abs/2501.03699>.

Richard Zhang, Phillip Isola, Alexei A Efros, Eli Shechtman, and Oliver Wang. The unreasonable effectiveness of deep features as a perceptual metric. In *Proceedings of the IEEE conference on computer vision and pattern recognition*, pages 586–595, 2018.

Shiwei* Zhang, Jiayu* Wang, Yingya* Zhang, Kang Zhao, Hangjie Yuan, Zhiwu Qing, Xiang Wang, Deli Zhao, and Jingren Zhou. I2vgen-xl: High-quality image-to-video synthesis via cascaded diffusion models, 2023.

Linqi Zhou, Aaron Lou, Samar Khanna, and Stefano Ermon. Denoising diffusion bridge models. In *The Twelfth International Conference on Learning Representations*, 2023.

Linqi Zhou, Aaron Lou, Samar Khanna, and Stefano Ermon. Denoising diffusion bridge models. In *The Twelfth International Conference on Learning Representations*, 2024a.

Shangchen Zhou, Peiqing Yang, Jianyi Wang, Yihang Luo, and Chen Change Loy. Upscale-A-Video: Temporal-consistent diffusion model for real-world video super-resolution. In *CVPR*, 2024b.

Time-Correlated Video Bridge Matching: Supplementary Materials

A PROOF OF PROPOSITIONS

Proof of Proposition 1. Consider the linear SDE

$$d\mathbf{X}_t = (\mathbf{A}\mathbf{X}_t + \mathbf{b})dt + \sqrt{\epsilon}d\mathbf{W}_t, \quad \mathbf{X}_0 \sim \delta_{\mathbf{X}_0},$$

with $\mathbf{A} \in \mathbb{R}^{D \times D}$ symmetric and invertible, $\mathbf{b} \in \mathbb{R}^D$, and a D -dimensional standard Wiener process \mathbf{W}_t .

Conditional mean. Let $\Phi(t) := e^{\mathbf{A}t}$ and define $\mathbf{Y}_t := (\Phi(t))^{-1}\mathbf{X}_t = e^{-\mathbf{A}t}\mathbf{X}_t$ (note $\mathbf{Y}_0 = \mathbf{X}_0$).

$$\begin{aligned} d\mathbf{Y}_t &= d(e^{-\mathbf{A}t}\mathbf{X}_t) = e^{-\mathbf{A}t}d\mathbf{X}_t + d(e^{-\mathbf{A}t})\mathbf{X}_t = \\ &e^{-\mathbf{A}t}[(\mathbf{A}\mathbf{X}_t + \mathbf{b})dt + \sqrt{\epsilon}d\mathbf{W}_t] - \mathbf{A}e^{-\mathbf{A}t}\mathbf{X}_t dt = e^{-\mathbf{A}t}\mathbf{b}dt + \sqrt{\epsilon}e^{-\mathbf{A}t}d\mathbf{W}_t, \end{aligned}$$

In the integral form:

$$\mathbf{Y}_t = \mathbf{X}_0 + \int_0^t e^{-\mathbf{A}s}\mathbf{b}ds + \sqrt{\epsilon} \int_0^t e^{-\mathbf{A}s}d\mathbf{W}_s.$$

Multiplying by $\Phi(t) = e^{\mathbf{A}t}$ yields:

$$\mathbf{X}_t = e^{\mathbf{A}t}\mathbf{X}_0 + \int_0^t e^{\mathbf{A}(t-s)}\mathbf{b}ds + \sqrt{\epsilon} \int_0^t e^{\mathbf{A}(t-s)}d\mathbf{W}_s. \quad (15)$$

Hence, the conditional mean is:

$$\boldsymbol{\mu}_{t|0}(\mathbf{X}_0) = e^{\mathbf{A}t}\mathbf{X}_0 + \left(\int_0^t e^{\mathbf{A}(t-s)}ds \right) \mathbf{b} = e^{\mathbf{A}t}\mathbf{X}_0 + (e^{\mathbf{A}t} - I)\mathbf{A}^{-1}\mathbf{b}, \quad (16)$$

Conditional variance.

$$\mathbf{I}_t := \int_0^t e^{\mathbf{A}(t-s)}d\mathbf{W}_s, \quad \text{so that} \quad \mathbf{X}_t - \boldsymbol{\mu}_{t|0}(\mathbf{X}_0) = \sqrt{\epsilon}\mathbf{I}_t.$$

$$\text{Cov}(\mathbf{X}_t \mid \mathbf{X}_0) = \mathbb{E}[(\mathbf{X}_t - \boldsymbol{\mu}_{t|0})(\mathbf{X}_t - \boldsymbol{\mu}_{t|0})^\top \mid \mathbf{X}_0] = \epsilon \text{Cov}(\mathbf{I}_t).$$

In turn:

$$\text{Cov}(\mathbf{I}_t) = \mathbb{E} \left[\left(\int_0^t e^{\mathbf{A}(t-s)}d\mathbf{W}_s \right) \left(\int_0^t e^{\mathbf{A}(t-r)}d\mathbf{W}_r \right)^\top \right].$$

By Itô isometry:

$$\mathbb{E} \left[\int_0^t G_s d\mathbf{W}_s \right] = 0, \quad \text{Cov} \left(\int_0^t G_s d\mathbf{W}_s, \int_0^t H_s d\mathbf{W}_s \right) = \int_0^t G_s H_s^\top ds.$$

Taking $G_s = H_s = e^{\mathbf{A}(t-s)}$ gives

$$\text{Cov}(\mathbf{I}_t) = \int_0^t e^{\mathbf{A}(t-s)} e^{\mathbf{A}^\top(t-s)} ds.$$

Because \mathbf{A} is symmetric, $e^{\mathbf{A}^\top u} = e^{\mathbf{A}u}$, hence

$$\text{Cov}(\mathbf{I}_t) = \int_0^t e^{2\mathbf{A}(t-s)} ds = \frac{1}{2}(e^{2\mathbf{A}t} - I)\mathbf{A}^{-1}.$$

Consequently,

$$\Sigma_{t|0} = \text{Cov}(\mathbf{X}_t \mid \mathbf{X}_0) = \frac{\epsilon}{2} (e^{2\mathbf{A}t} - \mathbf{I}) \mathbf{A}^{-1}.$$

Since $\mathbf{X}_t \mid \mathbf{X}_0$ is Gaussian with mean $\mu_{t|0}$ and covariance $\Sigma_{t|0}$, its score is

$$\nabla_{\mathbf{X}_t} \log q(\mathbf{X}_t \mid \mathbf{X}_0) = -\Sigma_{t|0}^{-1} (\mathbf{X}_t - \mu_{t|0}(\mathbf{X}_0)).$$

This completes the proof. \square

Proof of Proposition 2. **Step 1: Joint law from the prior.** From (15) and (16) in the proof of Proposition 1:

$$\mathbf{X}_u = \mu_{u|0}(\mathbf{X}_0) + \sqrt{\epsilon} \int_0^u e^{\mathbf{A}(u-s)} d\mathbf{W}_s,$$

$$\mu_{u|0}(\mathbf{X}_0) = e^{\mathbf{A}u} \mathbf{X}_0 + (e^{\mathbf{A}u} - \mathbf{I}) \mathbf{A}^{-1} \mathbf{b}.$$

Thus, conditionally on \mathbf{X}_0 ,

$$\mathbb{E}[\mathbf{X}_t \mid \mathbf{X}_0] = \mu_{t|0}(\mathbf{X}_0), \quad \mathbb{E}[\mathbf{X}_{t'} \mid \mathbf{X}_0] = \mu_{t'|0}(\mathbf{X}_0),$$

$$\Sigma_{t|0} = \frac{\epsilon}{2} (e^{2\mathbf{A}t} - \mathbf{I}) \mathbf{A}^{-1}, \quad \Sigma_{t'|0} = \frac{\epsilon}{2} (e^{2\mathbf{A}t'} - \mathbf{I}) \mathbf{A}^{-1}.$$

For the cross-covariance, using Itô isometry and independence of increments, for $t < t'$,

$$\Sigma_{t,t'|0} = \text{Cov}(\mathbf{X}_t, \mathbf{X}_{t'} \mid \mathbf{X}_0) = \epsilon \int_0^t e^{\mathbf{A}(t-s)} e^{\mathbf{A}(t'-s)} ds = \epsilon \int_0^t e^{\mathbf{A}(t+t'-2s)} ds = \frac{\epsilon}{2} \mathbf{A}^{-1} (e^{\mathbf{A}(t+t')} - e^{\mathbf{A}(t'-t)}).$$

Collecting blocks, we have the joint Gaussian (conditionally on X_0)

$$\begin{bmatrix} \mathbf{X}_t \\ \mathbf{X}_{t'} \end{bmatrix} \sim \mathcal{N} \left(\begin{bmatrix} \mu_{t|0}(\mathbf{X}_0) \\ \mu_{t'|0}(\mathbf{X}_0) \end{bmatrix}, \begin{bmatrix} \Sigma_{t|0} & \Sigma_{t,t'|0} \\ \Sigma_{t,t'|0} & \Sigma_{t'|0} \end{bmatrix} \right).$$

Step 2: Conditioning to obtain the bridge. For a joint Gaussian $\begin{bmatrix} x \\ y \end{bmatrix}$ with blocks $(\mu_x, \mu_y, \Sigma_{xx}, \Sigma_{yy}, \Sigma_{xy})$, the conditional $x \mid y$ is (Petersen et al., 2008, Section 8.1.3):

$$x \mid y \sim \mathcal{N}(\mu_x + \Sigma_{xy} \Sigma_{yy}^{-1} (y - \mu_y), \Sigma_{xx} - \Sigma_{xy} \Sigma_{yy}^{-1} \Sigma_{yx}).$$

Applying this with $x = \mathbf{X}_t$, $y = \mathbf{X}_{t'}$ and the blocks above gives:

$$\begin{aligned} \mu_{t|0,t'} &= \mu_{t|0}(\mathbf{X}_0) + \Sigma_{t,t'|0} \Sigma_{t'|0}^{-1} (\mathbf{X}_{t'} - \mu_{t'|0}(\mathbf{X}_0)), \\ \Sigma_{t|0,t'} &= \Sigma_{t|0} - \Sigma_{t,t'|0} \Sigma_{t'|0}^{-1} \Sigma_{t,t'|0}. \end{aligned}$$

Here

$$\Sigma_{t|0} = \frac{\epsilon}{2} (e^{2\mathbf{A}t} - \mathbf{I}) \mathbf{A}^{-1}, \quad \Sigma_{t'|0} = \frac{\epsilon}{2} (e^{2\mathbf{A}t'} - \mathbf{I}) \mathbf{A}^{-1}, \quad \Sigma_{t,t'|0} = \frac{\epsilon}{2} \mathbf{A}^{-1} (e^{\mathbf{A}(t+t')} - e^{\mathbf{A}(t'-t)}).$$

This completes the proof. \square

Proof of Proposition 3. Consider the following bijective reparameterization:

$$v_\phi(\mathbf{X}_t, t) = -\Sigma_{t|0}^{-1} (\mathbf{X}_t - \mu_{t|0}(\hat{\mathbf{X}}_0^\phi(\mathbf{X}_t, t)))$$

and substitute it in the optimization problem:

$$\min_\phi \mathbb{E}_{\mathbf{X}_0, \mathbf{X}_t, t} \left[\left\| v_\phi(\mathbf{X}_t, t) + \Sigma_{t|0}^{-1} (\mathbf{X}_t - \mu_{t|0}(\mathbf{X}_0)) \right\|^2 \right],$$

$$\begin{aligned}
 & \min_{\phi} \mathbb{E}_{\mathbf{X}_0, \mathbf{X}_t, t} \left[\left\| -\Sigma_{t|0}^{-1} \left(\mathbf{X}_t - \mu_{t|0}(\hat{\mathbf{X}}_0^\phi(\mathbf{X}_t, t)) \right) + \Sigma_{t|0}^{-1} (\mathbf{X}_t - \mu_{t|0}(\mathbf{X}_0)) \right\|^2 \right] = \\
 & \min_{\phi} \mathbb{E}_{\mathbf{X}_0, \mathbf{X}_t, t} \left[\left\| \Sigma_{t|0}^{-1} \left((\mathbf{X}_t - \mu_{t|0}(\mathbf{X}_0)) - (\mathbf{X}_t - \mu_{t|0}(\hat{\mathbf{X}}_0^\phi(\mathbf{X}_t, t))) \right) \right\|^2 \right] = \\
 & \min_{\phi} \mathbb{E}_{\mathbf{X}_0, \mathbf{X}_t, t} \left[\left\| \Sigma_{t|0}^{-1} \left(\mu_{t|0}(\hat{\mathbf{X}}_0^\phi(\mathbf{X}_t, t)) - \mu_{t|0}(\mathbf{X}_0) \right) \right\|^2 \right] = \\
 & \min_{\phi} \mathbb{E}_{\mathbf{X}_0, \mathbf{X}_t, t} \left[\left(\mu_{t|0}(\hat{\mathbf{X}}_0^\phi(\mathbf{X}_t, t)) - \mu_{t|0}(\mathbf{X}_0) \right)^\top (\Sigma_{t|0}^\top)^{-1} \Sigma_{t|0}^{-1} \left(\mu_{t|0}(\hat{\mathbf{X}}_0^\phi(\mathbf{X}_t, t)) - \mu_{t|0}(\mathbf{X}_0) \right) \right]
 \end{aligned}$$

Taking the gradient of this objective with respect to ϕ , we obtain:

$$\mathbb{E}_{\mathbf{X}_0, \mathbf{X}_t, t} \left[2(\Sigma_{t|0}^\top)^{-1} \Sigma_{t|0}^{-1} \left(\mu_{t|0}(\hat{\mathbf{X}}_0^\phi(\mathbf{X}_t, t)) - \mu_{t|0}(\mathbf{X}_0) \right) \right] = 0$$

Since $\Sigma_{t|0}^{-1}$ is positive definite we can multiply by $\frac{1}{2} \Sigma_{t|0} (\Sigma_{t|0}^\top)$ and get:

$$\mathbb{E}_{\mathbf{X}_0, \mathbf{X}_t, t} \left[\mu_{t|0}(\hat{\mathbf{X}}_0^\phi(\mathbf{X}_t, t)) - \mu_{t|0}(\mathbf{X}_0) \right] = 0$$

Then for each \mathbf{X}_t consider conditional mean:

$$\mathbb{E}_{\mathbf{X}_t, t} \left[\mathbb{E}_{\mathbf{X}_0 | \mathbf{X}_t} \left[\mu_{t|0}(\hat{\mathbf{X}}_0^\phi(\mathbf{X}_t, t)) - \mu_{t|0}(\mathbf{X}_0) \right] \right] = 0$$

$$\mathbb{E}_{\mathbf{X}_0 | \mathbf{X}_t} \left[\mu_{t|0}(\hat{\mathbf{X}}_0^\phi(\mathbf{X}_t, t)) - \mu_{t|0}(\mathbf{X}_0) \right] = 0$$

From (16) we have:

$$\mu_{t|0}(\mathbf{X}_0) = e^{\mathbf{A}t} \mathbf{X}_0 + \left(\int_0^t e^{\mathbf{A}(t-s)} ds \right) \mathbf{b} = e^{\mathbf{A}t} \mathbf{X}_0 + (e^{\mathbf{A}t} - I) \mathbf{A}^{-1} \mathbf{b},$$

Then (note that $e^{\mathbf{A}t}$ is invertible and we can multiplu both sides on e^{-At}):

$$\begin{aligned}
 & \mathbb{E}_{\mathbf{X}_0 | \mathbf{X}_t} \left[e^{\mathbf{A}t} \mathbf{X}_0^\phi(\mathbf{X}_t, t) + (e^{\mathbf{A}t} - I) \mathbf{A}^{-1} \mathbf{b} - e^{\mathbf{A}t} \mathbf{X}_0 + (e^{\mathbf{A}t} - I) \mathbf{A}^{-1} \mathbf{b} \right] = 0 \\
 & \mathbb{E}_{\mathbf{X}_0 | \mathbf{X}_t} \left[e^{\mathbf{A}t} (\mathbf{X}_0^\phi(\mathbf{X}_t, t) - \mathbf{X}_0) \right] = 0 \\
 & \mathbb{E}_{\mathbf{X}_0 | \mathbf{X}_t} \left[\mathbf{X}_0^\phi(\mathbf{X}_t, t) - \mathbf{X}_0 \right] = 0 \\
 & \mathbf{X}_0^\phi(\mathbf{X}_t, t) = \mathbb{E}_{\mathbf{X}_0 | \mathbf{X}_t} [\mathbf{X}_0]
 \end{aligned}$$

Hence, optimal $\mathbf{X}_0^* = \mathbb{E}_{\mathbf{X}_0 | \mathbf{X}_t} [\mathbf{X}_0]$, which in turn is the minimizer of MSE problem:

$$\min_{\phi} \mathbb{E}_{\mathbf{X}_0, \mathbf{X}_t, t} \left[\left\| \hat{\mathbf{X}}_0^\phi(\mathbf{X}_t, t) - \mathbf{X}_0 \right\|^2 \right].$$

By substituting in to v_ϕ we have:

$$v^*(\mathbf{X}_t, t) = -\Sigma_{t|0}^{-1} \left(\mathbf{X}_t - \mu_{t|0}(\hat{\mathbf{X}}_0^*(\mathbf{X}_t, t)) \right)$$

This completes the proof. \square

B ADDITIONAL QUANTITATIVE RESULTS

Here, we present the results of a quantitative comparison between DDPM, DDIM, Bridge Matching (BM), and our proposed method, TCVBM. The values of the standard deviation are provided, based on 3 runs of each method with different random seeds.

Table 4: Frame interpolation quantitative results with standard deviation. The best values in column are bold, second best values are underlined.

Metric	FVD \downarrow	LPIPS \downarrow	PSNR \uparrow	SSIM \uparrow
DDIM	34.664 ± 5.80	0.120 ± 0.070	15.843 ± 0.120	0.766 ± 0.011
DDPM	<u>33.612 ± 1.494</u>	0.107 ± 0.009	14.509 ± 0.427	0.714 ± 0.024
BM	34.766 ± 0.398	<u>0.078 ± 0.001</u>	<u>17.265 ± 0.390</u>	<u>0.789 ± 0.005</u>
TCVBM (ours)	31.491 ± 4.035	0.071 ± 0.019	17.451 ± 0.459	0.825 ± 0.044

Table 5: Image-to-Video generation quantitative results with standard deviation. The best values in column are bold, second best values are underlined.

Metric	FVD \downarrow	LPIPS \downarrow	PSNR \uparrow	SSIM \uparrow
DDIM	335.51 ± 241.12	0.402 ± 0.092	10.205 ± 0.514	0.513 ± 0.069
DDPM	250.52 ± 134.99	0.383 ± 0.054	10.333 ± 0.275	0.530 ± 0.046
BM	<u>48.54 ± 0.56</u>	<u>0.268 ± 0.005</u>	<u>10.627 ± 0.053</u>	<u>0.582 ± 0.004</u>
TCVBM (ours)	45.32 ± 0.91	0.260 ± 0.002	10.710 ± 0.028	0.589 ± 0.001

Table 6: Video super resolution quantitative results with standard deviation. The best values in column are bold, second best values are underlined.

Metric	FVD \downarrow	LPIPS \downarrow	PSNR \uparrow	SSIM \uparrow
DDIM	336.808 ± 5.175	0.520 ± 0.006	17.226 ± 0.103	0.600 ± 0.016
DDPM	614.288 ± 6.289	0.237 ± 0.001	20.152 ± 0.050	0.577 ± 0.004
BM	<u>29.710 ± 20.683</u>	<u>0.026 ± 0.005</u>	<u>21.412 ± 1.040</u>	<u>0.941 ± 0.012</u>
TCVBM (ours)	<u>32.762 ± 23.153</u>	<u>0.029 ± 0.004</u>	21.431 ± 1.419	0.941 ± 0.011

C INITIALIZATION EXPERIMENTS

In this section, we explore options for initializing or representing input data for bridge-based methods used in our work, namely for Bridge Matching with Browninan Bridge (BM) and Time-Correlated Video Bridge Matching (TCVBM). The interest in initialization is primarily due to the fact that presumably these methods are better suited to data-to-data translation tasks. The interest in exploring the effect of input data initialization on the quality of model performance stems primarily from the assumption that bridge-based approaches are better suited for data-to-data translation tasks.

C.1 Frame Interpolation

As input data for the network, we explored two options: filling in intermediate frames with Gaussian noise sampled from $\mathcal{N}(\mathbf{0}, \mathbf{1})$ and using linear interpolation between fixed boundary frames \mathbf{x}^0 and \mathbf{x}^N , i.e.:

$$\mathbf{x}_{input}^n = \frac{n\mathbf{x}^0 + (N-n)\mathbf{x}^N}{N}, \quad n = 1, \dots, N-1.$$

Table 7 compares the results of these initialization methods. As can be seen, filling intermediate frames with noise from a normal distribution produces better results than the initial linear interpolation.

Table 7: Analysis of the impact of initialization of input video data for bridge-based methods in the task of frame interpolation. Using noise from a normal distribution shows a clear advantage. The best values in column are bold, second best values are underlined.

Initialization method	Method	FVD ↓	LPIPS ↓	PSNR ↑	SSIM ↑
Linear interpolation	BM	34.804	0.109	15.439	0.756
	TCVBM	<u>31.944</u>	0.092	16.275	0.782
Gaussian noise from $\mathcal{N}(0, 1)$	BM	34.315	<u>0.079</u>	<u>17.103</u>	0.794
	TCVBM	30.542	0.077	17.280	0.813

C.2 Image-to-Video Generation

Here we compare the following two types of initial initialization: duplicating the first frame in place of the frames to be generated (static video) and using random noise everywhere except the first frame. Static video initialization is superior to the noise option for both models (Table 8).

Table 8: Comparison of two types of initial initialization of input data for image-to-video generation.

Initialization method	Method	FVD ↓	LPIPS ↓	PSNR ↑	SSIM ↑
Static video	BM	49.32	0.271	10.63	0.579
	TCVBM	44.96	0.258	10.75	0.591
Gaussian noise from $\mathcal{N}(0, 1)$	BM	52.57	0.287	10.61	0.568
	TCVBM	<u>48.61</u>	<u>0.263</u>	<u>10.68</u>	<u>0.587</u>

C.3 Video Super Resolution

Table 9: Comparison of two types of initial initialization of input data for video super resolution. We perform this comparison for low-resolution 32×32 .

Initialization method	Method	FVD ↓	LPIPS ↓	PSNR ↑	SSIM ↑
Low-resolution video	BM	<u>9.501</u>	<u>0.014</u>	24.888	<u>0.972</u>
	TCVBM	9.496	0.012	24.970	0.973
Low-resolution video concatenated with noise from $\mathcal{N}(0, 1)$	BM	9.556	0.012	<u>24.892</u>	0.973
	TCVBM	9.646	0.012	24.988	0.973

D HYPERPARAMETERS SEARCHING

Here we compare different values of hyperparameters, namely the noise scaling value ϵ and the coefficient α , which determines the degree of impact of the matrix \mathbf{A} as $\tilde{\mathbf{A}} := \alpha \mathbf{A}$. Table 10 shows that in the case of frame interpolation, it is impossible to identify a clear dependence of the generation quality on the hyperparameters used, however, a sufficient amount of noise and not large values for the α coefficient are optimal. The results for video super resolution in Table 11 demonstrate that small values of ϵ and α are optimal for this task, which does not contradict the results for frame interpolation.

Table 10: The results of TCVBM training with various hyperparameters ϵ and α for frame interpolation. The best values in column are bold, second best values are underlined.

ϵ	α	FVD ↓	LPIPS ↓	PSNR ↑	SSIM ↑
0.1	0.1	35.572	0.085	16.40	0.797
0.1	1	36.542	0.089	16.37	0.797
0.1	10	<u>29.792</u>	0.086	16.56	0.801
1	0.1	27.342	0.084	16.65	0.803
1	1	30.542	0.077	16.86	0.813
1	10	31.432	<u>0.080</u>	17.12	0.817
10	0.1	37.662	0.084	17.24	0.819
10	1	54.542	0.093	<u>17.17</u>	0.818
10	10	54.562	0.100	<u>17.17</u>	0.769

Table 11: The results of TCVBM training with various hyperparameters ϵ and α for video super resolution. We perform this comparison for low-resolution 32×32 .

ϵ	α	FVD ↓	LPIPS ↓	PSNR ↑	SSIM ↑
0.1	0.1	9.496	0.012	24.970	0.973
0.1	1	<u>10.413</u>	<u>0.013</u>	<u>24.358</u>	<u>0.969</u>
1	0.1	13.226	0.019	23.004	0.959
1	1	15.023	0.022	22.120	0.949
10	0.1	18.458	0.033	20.085	0.921
10	1	20.746	0.039	19.283	0.906

E DYNAMICAL CORRELATION

E.1 Theory

Consider prior SDE with an additional multiplicative function $f(t)$ depending only on time t :

$$d\mathbf{X}_t = f(t)(\mathbf{A}\mathbf{X}_t + \mathbf{b})dt + \sqrt{\epsilon}d\mathbf{W}_t.$$

The derivation of formulas for this prior follows the same principles used for $f(t) = 1$ in Appendix A.

Define:

$$F(t) = \int_0^t f(\tau) d\tau, \quad \Phi(t) = e^{\mathbf{A}F(t)}.$$

Then $\frac{d}{dt}\Phi(t) = f(t)\mathbf{A}\Phi(t)$, $\Phi(0) = I$, and $\frac{d}{dt}\Phi(t)^{-1} = -f(t)\Phi(t)^{-1}\mathbf{A}$.

Conditional mean. Consider $\mathbf{Y}_t := \Phi(t)^{-1}\mathbf{X}_t$. By Itô's rule:

$$\begin{aligned} d\mathbf{Y}_t &= \Phi(t)^{-1}d\mathbf{X}_t + d(\Phi(t)^{-1})\mathbf{X}_t = \Phi(t)^{-1}f(t)(\mathbf{A}\mathbf{X}_t + \mathbf{b})dt + \sqrt{\epsilon}\Phi(t)^{-1}d\mathbf{W}_t - f(t)\Phi(t)^{-1}\mathbf{A}\mathbf{X}_t dt = \\ &= \Phi(t)^{-1}f(t)\mathbf{b}dt + \sqrt{\epsilon}\Phi(t)^{-1}d\mathbf{W}_t. \end{aligned}$$

Integrating from 0 to t gives

$$\mathbf{Y}_t = \mathbf{X}_0 + \int_0^t \Phi(s)^{-1}f(s)\mathbf{b}ds + \sqrt{\epsilon} \int_0^t \Phi(s)^{-1}d\mathbf{W}_s,$$

and thus

$$\mathbf{X}_t = \Phi(t)\mathbf{X}_0 + \Phi(t) \int_0^t \Phi(s)^{-1}f(s)\mathbf{b}ds + \sqrt{\epsilon}\Phi(t) \int_0^t \Phi(s)^{-1}d\mathbf{W}_s.$$

Taking expectation and using $\Phi(t)\Phi(s)^{-1} = e^{\mathbf{A}(F(t)-F(s))}$,

$$\mu_{t|0}(\mathbf{X}_0) = \mathbb{E}[\mathbf{X}_t | \mathbf{X}_0] = e^{\mathbf{A}F(t)}\mathbf{X}_0 + \int_0^{F(t)} e^{\mathbf{A}(F(t)-F(s))}f(s)\mathbf{b}ds.$$

With the change of variables $u = F(s)$ (so $du = f(s)ds$) this equals

$$\int_0^{F(t)} e^{\mathbf{A}(F(t)-u)}du \mathbf{b} = \left[-e^{\mathbf{A}(F(t)-u)}\mathbf{A}^{-1} \right]_{u=0}^{F(t)} \mathbf{b} = (e^{\mathbf{A}F(t)} - I)\mathbf{A}^{-1}\mathbf{b}.$$

Therefore

$$\mu_{t|0}(\mathbf{X}_0) = e^{\mathbf{A}F(t)}\mathbf{X}_0 + (e^{\mathbf{A}F(t)} - I)\mathbf{A}^{-1}\mathbf{b}.$$

The mean $\mu_{t|0}(X_0)$ of the process starting from a given \mathbf{X}_0 is given by:

$$\mu_{t|0}(\mathbf{X}_0) = e^{\mathbf{A}F(t)}\mathbf{X}_0 + (e^{\mathbf{A}F(t)} - I)\mathbf{A}^{-1}\mathbf{b}.$$

Conditional variance. Let $\mathbf{Z}_t := \mathbf{X}_t - \mu_{t|0}$ be the centered process. Subtracting the mean SDE from the original SDE yields

$$d\mathbf{Z}_t = f(t)\mathbf{A}\mathbf{Z}_t dt + \sqrt{\epsilon}d\mathbf{W}_t.$$

Define the covariance $\Sigma_{t|0} := \mathbb{E}[\mathbf{Z}_t \mathbf{Z}_t^\top]$. Using Itô's rule for $\mathbf{Z}_t \mathbf{Z}_t^\top$,

$$d(\mathbf{Z}_t \mathbf{Z}_t^\top) = (d\mathbf{Z}_t)\mathbf{Z}_t^\top + \mathbf{Z}_t(d\mathbf{Z}_t)^\top + d\mathbf{Z}_t(d\mathbf{Z}_t)^\top,$$

where

$$(d\mathbf{Z}_t)\mathbf{Z}_t^\top = f(t)\mathbf{A}\mathbf{Z}_t \mathbf{Z}_t^\top dt + \sqrt{\epsilon}d\mathbf{W}_t \mathbf{Z}_t^\top, \quad (17)$$

$$\mathbf{Z}_t(d\mathbf{Z}_t)^\top = f(t)\mathbf{Z}_t \mathbf{Z}_t^\top \mathbf{A}^\top dt + \sqrt{\epsilon}\mathbf{Z}_t d\mathbf{W}_t^\top, \quad (18)$$

$$(d\mathbf{Z}_t)(d\mathbf{Z}_t)^\top = \epsilon d\mathbf{W}_t d\mathbf{W}_t^\top = \epsilon I dt. \quad (19)$$

Hence

$$d(\mathbf{Z}_t \mathbf{Z}_t^\top) = f(t) (\mathbf{A} \mathbf{Z}_t \mathbf{Z}_t^\top + \mathbf{Z}_t \mathbf{Z}_t^\top \mathbf{A}^\top) dt + \sqrt{\epsilon} d\mathbf{W}_t \mathbf{Z}_t^\top + \sqrt{\epsilon} \mathbf{Z}_t d\mathbf{W}_t^\top + \epsilon I dt.$$

and taking expectations gives

$$\frac{d}{dt} \Sigma_{t|0} = f(t) \mathbf{A} \Sigma_{t|0} + f(t) \Sigma_{t|0} \mathbf{A}^\top + \epsilon I, \quad \Sigma_{t|0} = 0.$$

To get the cross-covariance, we use:

$$\mathbf{Z}_t = \sqrt{\epsilon} \int_0^t e^{\mathbf{A}(F(t)-F(s))} d\mathbf{W}_s, \quad \mathbf{Z}_{t'} = \sqrt{\epsilon} \int_0^{t'} e^{\mathbf{A}(F(t')-F(u))} d\mathbf{W}_u,$$

The Itô isometry yields

$$\Sigma_{t,t'|0} := \text{Cov}(\mathbf{Z}_t, \mathbf{Z}_{t'}^\top) = \epsilon \int_0^t e^{\mathbf{A}(F(t)-F(s))} e^{\mathbf{A}(F(t')-F(s))^\top} ds.$$

For symmetric \mathbf{A} , $e^{(\cdot)^\top} = e^{(\cdot)}$ and, since these exponentials commute (all are $e^{\mathbf{A}(\cdot)}$),

$$e^{\mathbf{A}(F(t)-F(s))} e^{\mathbf{A}(F(t')-F(s))} = e^{\mathbf{A}(F(t')-F(t))} e^{2\mathbf{A}(F(t)-F(s))}.$$

Hence

$$\Sigma_{t,t'|0} = e^{\mathbf{A}(F(t')-F(t))} \epsilon \int_0^t e^{2\mathbf{A}(F(t)-F(s))} ds = e^{\mathbf{A}[F(t')-F(t)]} \Sigma_{t|0}.$$

Summary. Thus, all three components: mean $\mu_{t|0}(\mathbf{X}_0)$, variance $\Sigma_{t|0}$, and cross-covariance $\Sigma_{t,t'|0}$ are derived and can be used further in the same way as in the original case of $f(t) = 1$.

E.2 Experimental Results

The continuous and time-decreasing function $f(t)$ sets the increasing values of the matrix \mathbf{A} in the inverse diffusion process when $t \rightarrow 0$. Thus, the correlation of frames with each other in the generated video increases in the last steps of the inference. We conduct a series of experiments to investigate the effect of dynamic correlation and the choice of the function $f(t)$. We use the same experimental setting as described in Section 5.1 of the main paper, with a number of optimizer steps set to 120,000. The frame interpolation results are presented in Table 12. As can be seen, our experiments do not demonstrate the advantages of using dynamic correlation compared to using constant values of the matrix \mathbf{A} . However, we observe significant differences in the quality of the results depending on the function $f(t)$. This demonstrates a complex structure of the relationship between video frames in the diffusion process, which our framework provides in the constant linear approximation.

Table 12: The results of the selection of the function $f(t)$, which determines the inverse dependence of the values of the matrix \mathbf{A} on time t . The best values in column are bold, second best values are underlined.

$f(t)$	FVD \downarrow	LPIPS \downarrow	PSNR \uparrow	SSIM \uparrow
1 - t	49.569	0.115	13.938	<u>0.752</u>
1 - $2t$	398.823	0.202	11.760	0.684
1 - 0.5 t	427.942	0.226	12.063	0.620
$2 \times (1 - t)$	409.495	0.195	12.239	0.624
$0.5 \times (1 - t)$	269.899	0.182	12.297	0.676
$(1 - t)^2$	<u>43.651</u>	<u>0.112</u>	13.916	0.751
e^{-t}	1910.002	0.973	3.600	0.002
e^{-2t}	1216.250	0.629	7.243	0.119
e^{-4t}	108.052	0.142	13.186	0.688
e^{-8t}	50.078	0.128	13.321	0.726
Constant ($f(t) = \alpha = 1$)	36.309	0.097	14.515	0.772

F ADDITIONAL VISUAL EXAMPLES

F.1 Frame Interpolation

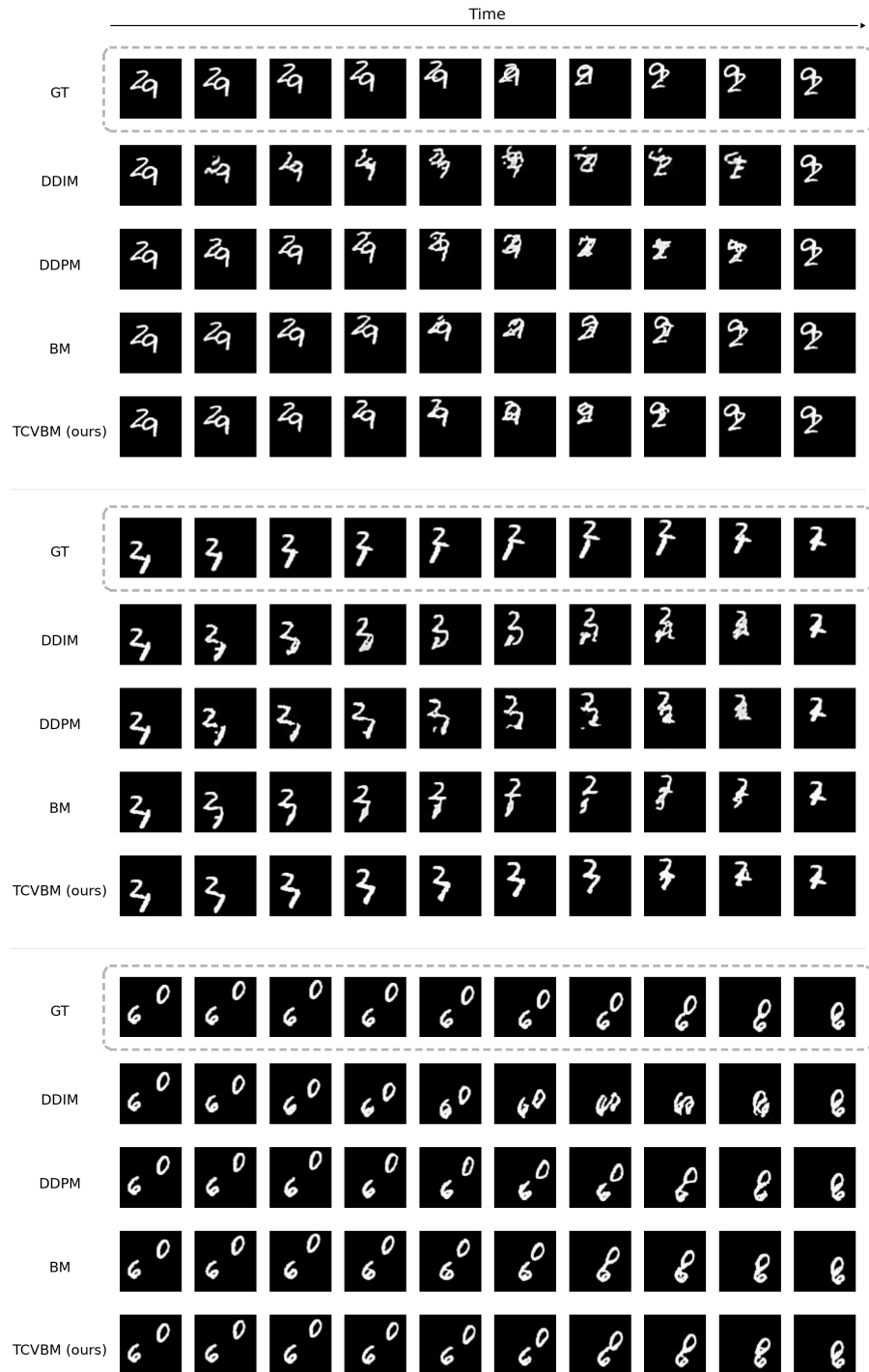


Figure 5: Additional frame interpolation results.

F.2 Image-to-Video Generation

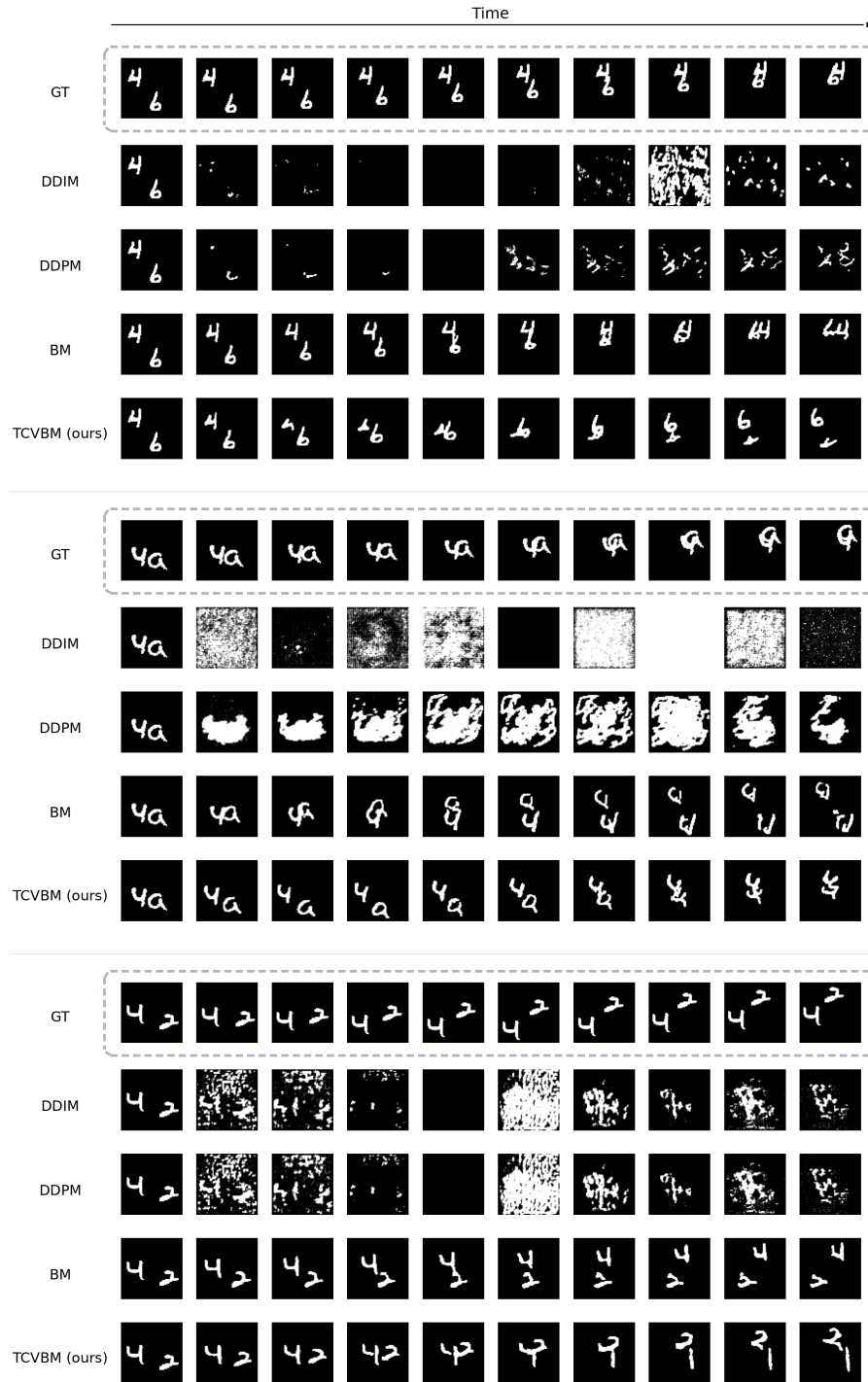


Figure 6: Additional image-to-video results.

F.3 Video Super Resolution

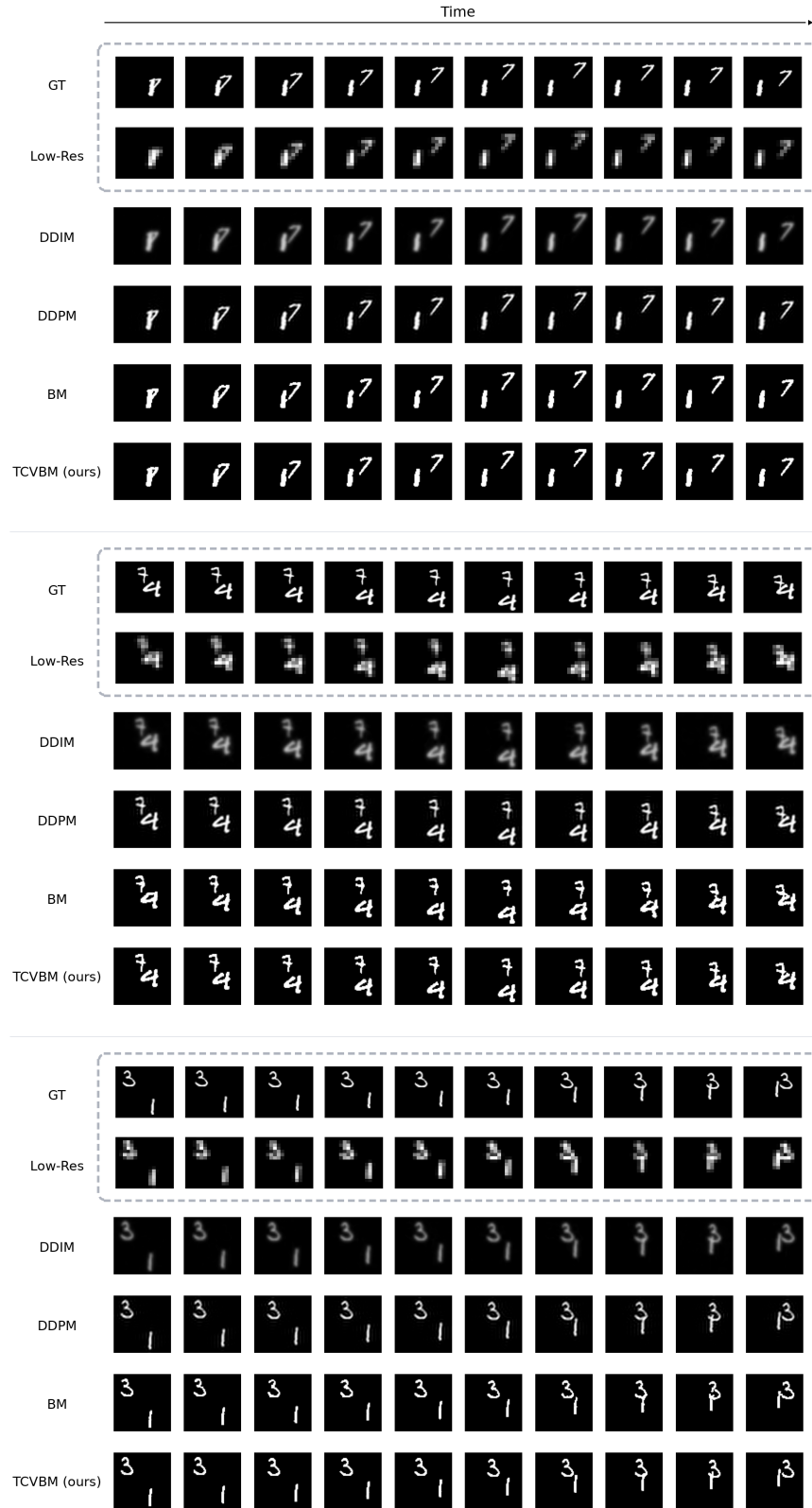


Figure 7: Additional video super resolution results. The resolution is increased from 16×16 to 64×64 .